Supplementary Materials for

Release of Mineral-Bound Water Prior to Subduction Tied to Shallow Seismogenic Slip off Sumatra

Andre Hüpers, Marta E. Torres, Satoko Owari, Lisa C. McNeill, Brandon Dugan, Timothy J. Henstock, Kitty L. Milliken, Katerina E. Petronotis, Jan Backman, Sylvain Bourlange, Farid Chemale, Jr., Wenhuang Chen, Tobias A. Colson, Marina C.G. Frederik, Gilles Guèrin, Mari Hamahashi, Brian M. House, Tamara N. Jeppson, Sarah Kachovich, Abby R. Kenigsberg, Mebae Kuranaga, Steffen Kutterolf, Freya L. Mitchison, Hideki Mukoyoshi, Nisha Nair, Kevin T. Pickering, Hugo F.A. Pouderoux, Yehua Shan, Insun Song, Paola Vannucchi, Peter J. Vrolijk, Tao Yang, Xixi Zhao

correspondence to: ahuepers@uni-bremen.de

This PDF file includes:

Materials and Methods

Interstitial water analyses

Interstitial water samples were collected onboard R/V JOIDES Resolution from whole-round sections that were cut from the sediment cores immediately after recovery. The interstitial water was extracted with a Manheim-type titanium squeezer using loading stresses of up to 24.5 MPa at ambient temperatures (*32*). In smectite-rich sediment stress-induced release of interlayer water on the order of up to ~7 wt.-% smectite may cause a freshening artifact from laboratory squeezing starting at 1.3 MPa effective stress (*33*). Due to the high hydrostatic effective stress of 14 MPa (*16*) we infer that the observed freshening is not influenced by laboratory squeezing of smectite minerals. Chloride concentrations were acquired using a Metrohm 785 DMP auto-titrator and silver nitrate ($AgNO_3$) solutions that were calibrated against repeated titrations of an IAPSO standard, with a precision better than 0.3%. A 0.1 ml sample aliquot, diluted with 10 ml of 90 ± 2mM HNO_3, was titrated with a 0. 014N $AgNO_3$. Dissolved silica was measured by spectrophotometry using the reduction of a silicomolydate complex with ascorbic acid, and the absorbance of the resulting molybdenum blue was measured at 812 nM using an Agilent Technologies Cary Series 100 UV-Vis spectrophotometer. Calibration was done against dilutions of a 3000 µM (0.5642 g Na_2SiF_6 in 1L) silica primary standard ranging from 30 to 1200 µM.

Amorphous silica extractions

The silica extraction procedure employed is based on the one described by Lyle and Lyle (*18*), which was designed to quantify biogenic silica in radiolarian-rich Eocene sediment. As described by these authors, the commonly used 2M Na_2CO_3 extraction solution does not fully dissolve the biogenic opal in Eocene-Paleocene samples because these fossil assemblages are larger and thicker than the Neogene opal counterparts; therefore Lyle and Lyle (*18*) recommend the use of a 2M KOH solution. This reagent dissolves biogenic opal as well as volcanic glass and other amorphous silica phases, but does not dissolve significant amounts of SiO_2 from clay minerals or quartz (*18*).

For samples from Site U1480, we weighed 30 mg of freezed-dried, ground sediment sample and placed it in a 50-mL Corning CentriStar™ centrifuge tube to which 20 mL 2M KOH was added. Tubes were capped, mixed for 30 seconds with a vortex mixer and placed in a water bath at 85°C. We collected aliquots of the extract liquid at various time intervals (from 5 min to 24 hrs) after the digestion began. The samples were vortex mixed after each aliquot was drawn. The extract liquid was analyzed for dissolved silica using the method based on the production of a yellow silicomolybdate complex, by drawing 10-200 µL aliquots after the solution cooled. The silicomolybdate complex was reduced by ascorbic acid to form molybdenum blue (*34*), which was measured at 812 nm with an Agilent Technologies Cary Series 100 UV-Vis spectrophotometer. Results from replicate (n=2, 3) analyses of two samples from different lithologic units yielded concentrations that agreed within 2% in all the leaching steps.

X-Ray diffraction analyses

For XRD measurements bulk sediment samples (~5 cm^3) were vacuum dried, crushed for 3 minutes with a ball mill, and mounted as randomly oriented bulk powders. XRD analyses were performed using a Bruker D4 Endeavor diffractometer with CuKα1 (1.54060 Å) and CuKα2 (1.54443 Å) radiation at 40 kV and 40 mA over a scanning range of 2°–40°2θ, and at a step size of 0.008°2θ and a scan step time of 0.648 s. Identification of mineral phases was determined using the Bruker software package DIFFRAC EVA.

Diffusion model

The diffusion of an interstitial solute *[C]* in a water-saturated, 1-dimensional sediment column can be described by the following differential equation (*35*):

$$n \cdot \frac{\partial [C]}{\partial t} = \frac{\partial (n \cdot D_S \cdot \frac{\partial [C]}{\partial z})}{\partial z} \quad (1)$$

where n is fractional porosity and D_S is the diffusion coefficient of the solute (D_0) corrected for the tortuosity [$\Theta = 1\text{-}\ln(n^2)$] (*36*):

$$D_S = \frac{D_0}{1-\ln(n^2)} \quad (2)$$

We calculated D_0 for chloride after Boudreau (*37*) using a uniform thermal gradient of ~44.4°C/km as constrained at Site U1480 (*16*). The following modification of the Hubbert and Rubey (*38*) empirical relationship has been fitted to shipboard measured moisture and density porosity measurements (figure S5) of clay-rich samples to describe fractional porosity reduction with depth below seafloor (*z)*:

$$n = n_a \cdot e^{(-\alpha \cdot z)} + n_b \cdot e^{(-\beta \cdot z)} \quad (3)$$

in which the sum of n_a= 0.27 and n_b = 0.49 is the porosity at the seafloor and α=0.03 and β=0.0024 are the respective empirical attenuation constants, which provides R^2= 0.88.

Kinetic dehydration model

To investigate dewatering by compaction and mineral dehydration we track the depth and temperature conditions at the bottom of unit III in a 1-dimensional column as it approaches the deformation front with a constant subduction rate (v = 0.05 m/yr). Our model begins with the deposition of the basal unit III strata approximately ~38 Myr ago and simulates the sediment evolution 6.4 Myr into the future, coincident with arrival of the Site U1480 sediment column at the deformation front assuming that the sediment approaches the deformation front at an angle of ~45° (Fig. 1). With each time step (dt = 20 kyr; equivalent to 1 km advance in convergence direction) the thickness dz is added to the sediment column according to the sedimentation rate r:

$$dz = dt \cdot r \quad (4)$$

Age-depth relationships from biostratigraphic and biochronologic data from retrieved cores revealed linear sedimentation rates of up to 4 m/Myr for unit III and up to 362 m/Myr for the Nicobar fan sediments (*16*). We used an average sedimentation rate of r = 2.6 m/Myr for the sedimentation of unit III and r = 139 m/Myr for the deposition of the Nicobar Fan sediment. The subsequent burial beneath the trench wedge facies has been modeled with an average rate of r = 419 m/Myr and 575 m/Myr leading to a final burial depth of ~4 and 5 km for the base of unit III, respectively, consistent with the sediment thickness estimated from seismic reflection images (*14*).

For each step we calculated the release of mineral-bound water by the temperature-driven smectite to illite and opal-A/CT-quartz transitions. The smectite to illite transition is used as a proxy for palagonite dehydration because there is no data available for palagonite kinetics; however dehydration of smectite itself will also contribute to the fluid production. The temperature (T) was computed after Bullard (*38*) assuming thermal equilibrium:

$$T = T_0 + \frac{q}{\int_0^z \frac{dz}{k(z)}} \quad (5)$$

where T_0 is the seafloor temperature (1.2°C), q is heat flow and k is thermal conductivity. We determined the decline in heat flow q of the oceanic crust using the square root-time relation of Parsons and Sclater (*39*) and an initial value of 510 mW/m^2 (*40*), thus allowing for cooling of the ageing oceanic crust before the deposition of unit III:

$$q = \frac{510}{\sqrt{t}} \quad (6)$$

From the 11 borehole measurements in the upper 200 m below seafloor that yielded a linear geothermal gradient of 44.4°C/km (*16*), a temperature within the basal pelagic U1480 sediments of ~60°C is predicted. Initial model results underpredicted the temperature of 58.9°C at the base of unit III, therefore to match the temperature profile at Site U1480 we fixed the heat flow at a value of 72.6 mW/m^2 about 18.8 Myr before the sediment column reaches the modern-day location of Site U1480. The fixed heat flow honors the observed shift towards younger ages of the oceanic crust towards the deformation front (*41*). For the thermal conductivity we employed a linear relationship $k(z) = 5.6109 \cdot 10^4 \cdot z + 1.3436$ ($R^2 = 0.40$) to account for its increase with depth based on shipboard measured values of clay-rich samples with thermal conductivities ranging between 1.10 and 2.63 W/(m · K) (*16*). Two data points outside of the 95% confidence ellipse were excluded (at 1164.0 and 1243.3 meters below seafloor with thermal conductivities of 3.8 and 4.5 W/(m · K), respectively).

The kinetic reaction processes are updated in each step using estimates for new temperature *T*. The smectite-illite reaction is described after Huang (*19*) as:

$$\frac{dS}{dt} = -A_S \cdot exp^{-\frac{E_S}{RT}} \cdot [K]^+ \cdot S^2 \quad (7)$$

where the change in smectite mole fraction in mixed layer illite–smectite (S) is a function of temperature (Kelvin) and exposure time (t); A_S is a pre-exponential scaling factor ($8.08 \cdot 10^4$ s^{-1}), E_S is the activation energy ($1.17 \cdot 10^5$ J·mol^{-1}) and R is the gas constant. We assume a constant value of $[K]^+ = 2$ mM equal to measured pore water concentrations of dissolved potassium in the depth interval of the observed fluid freshening. The fluid production rate from the smectite-illite reaction kinetics is given by (*42*):

$$L = \frac{dS}{dt} \cdot H \cdot C_S \cdot (1 - n) \quad (8)$$

in which H is the water content in smectite (ca. 40 vol.-%) and C_S is the volume content of smectite in the bulk sediment. We tested values of $C = 50$ vol.-% and $C = 100$ vol.-% assuming the average smectite density to be similar to the bulk grain density (ca. 2.7 g/cm^3).

The dehydration of biogenic silica (opal-A) is a two-step process in which opal-A is transformed to quartz via opal-CT (*20*). We calculated the molar fraction of opal-A in opal-A/opal-CT (OA) by (*20*):

$$\frac{dOA}{dt} = -A_{OA} \cdot exp^{-\frac{E}{RT}} \cdot OA \quad (9)$$

and the molar fraction of opal-CT in opal-CT/quartz (*OCT*) by (*20*):

$$\frac{dOCT}{dt} = -A_{OCT} \cdot exp^{-\frac{E}{RT}} \cdot OCT \quad (10)$$

where A_{OA} = 7.51·10^{-4} s^{-1} , A_{OCT}=2.3·10^{-3} s^{-1} and E = 6.69·10^{5} J·mol^{-1}, respectively (*20*).

The fluid production rate from the two reactions above is given by (*43*):

$$L = C_{OA} \cdot (1 - n) \cdot \left(\frac{dOA}{dt} \cdot (H_{OA} - H_{OA}) + \frac{dOCT}{dt} \cdot \left(H_{OCT} - H_{QTZ}\right)\right) \quad (11)$$

in which C_{OA} is the initial volume content of opal-A in the bulk sediment and H is the volume content of water in opal-A (H_{OA}= 5 - 29.1 vol.-%), opal-CT (H_{OCT}= 2.4 - 21.4 vol.-%) and quartz (H_{QTZ}= 0.2 - 1.7 vol.-%), based on previously measured water contents by weight of 2.1 - 12.1 wt.-% for opal-A, 1 - 8.9 wt.-% for opal-CT, and 0.1 - 0.7 wt.-% for quartz (*22*) and an average density of 2.4 g/cm^3 (*44*).

The fluid production from compaction in unit III has been estimated from the rate of porosity loss per unit volume between each step:

$$L = \frac{dn}{dt} \quad (12)$$

where *dn* is the change in porosity of the fluid releasing layer that we obtained in each step from equation (3).

Supplementary Text

Comparison with other Subduction Zone Margins

Table S1 compiles parameters from a range of subduction zone margins comparable with North Sumatra, both with and without ground truth from ocean drilling and with and without good historic plate boundary earthquake records. These parameters relate to the input sediment thickness and depth of the initial décollement, the thermal state of the outer décollement, ocean drilling and evidence for early diagenesis, knowledge of plate boundary earthquakes and whether shallow slip has occurred, and the current proposed models for diagenesis and for earthquake slip style.

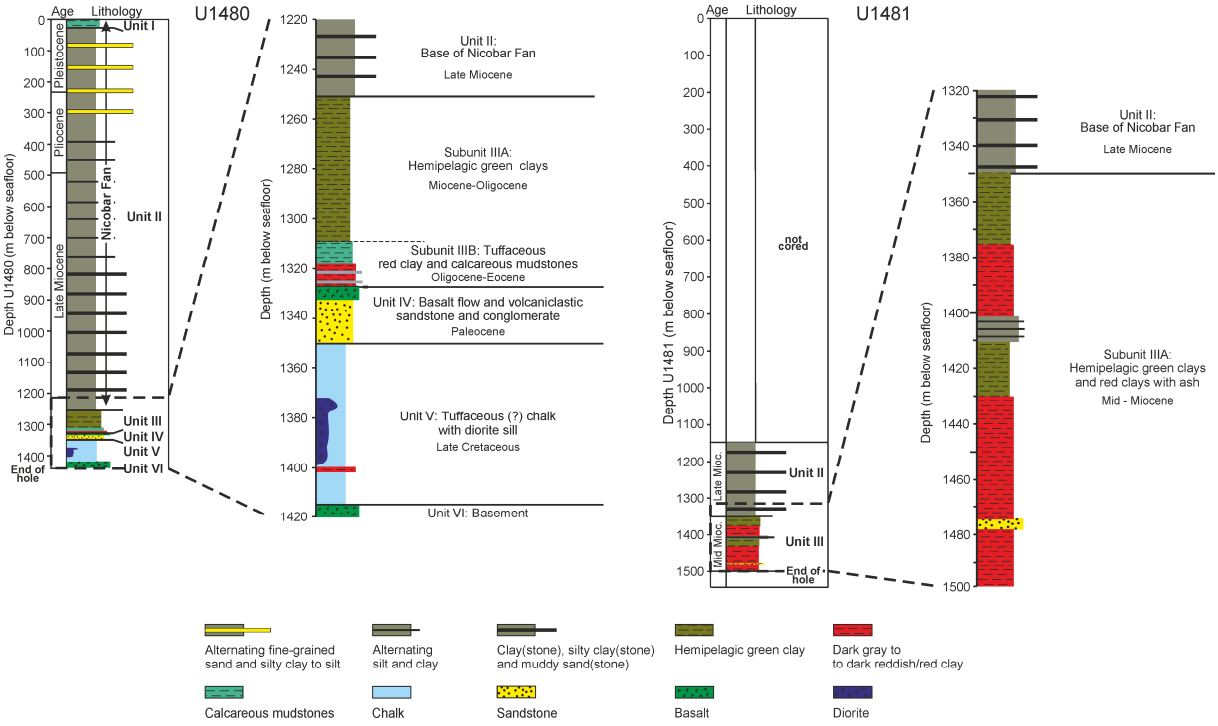

Fig. S1. Lithostratigraphy of Sites U1480 and U1481.

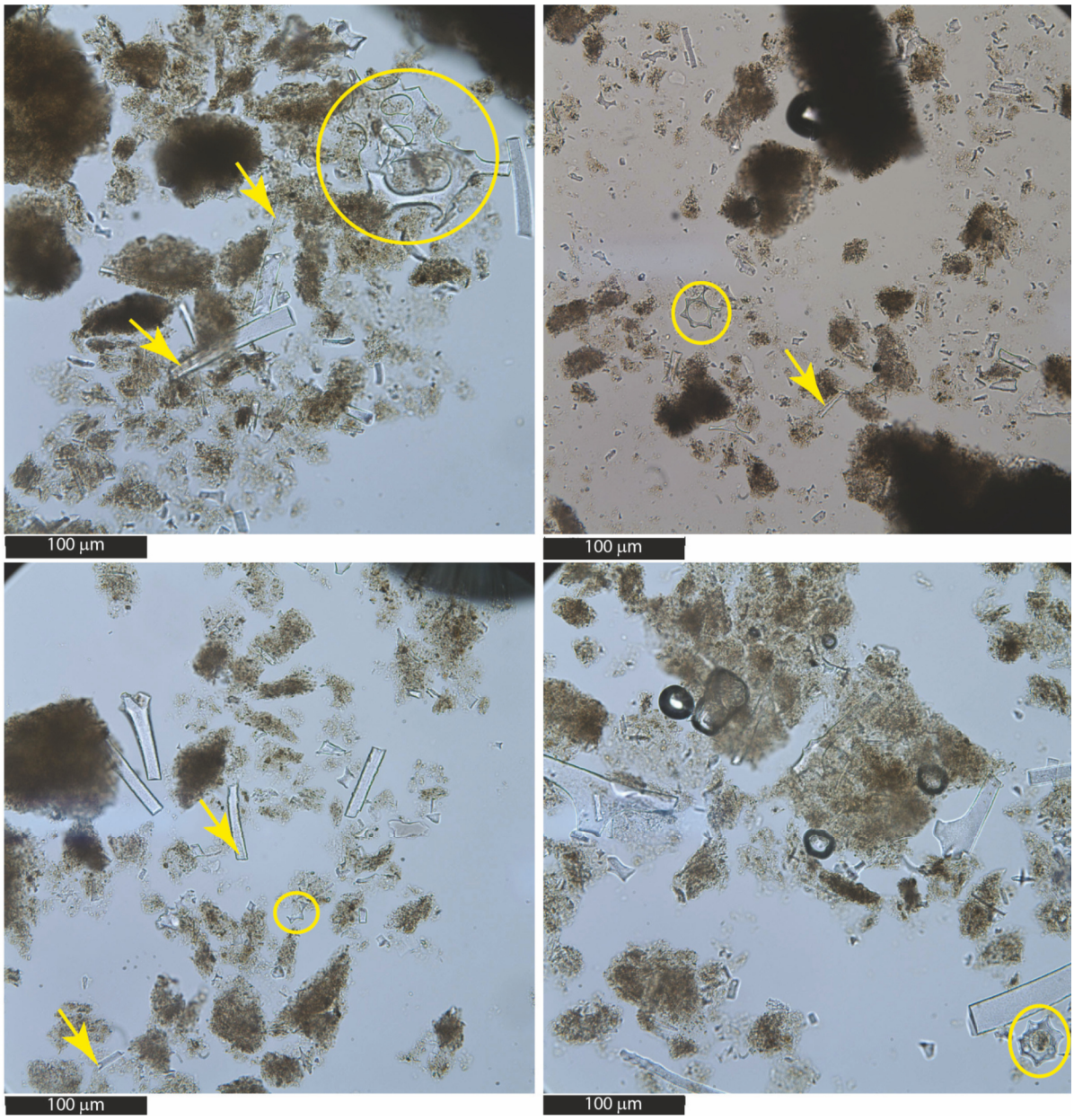

Fig. S2. Smear slide photomicrographs in transmitted plane-polarized light showing sediment components of the red-brown palagonite from subunit IIIB (Site U1480, 1325m below seafloor). Brownish to tan material is a mostly isotropic mix of clay minerals, oxides, and amorphous silicate (based on color and XRD character). Elongate translucent fragments are mostly sponge spicules. Yellow arrow indicates a spicule displaying a clear central canal. Yellow ovals denote fragments of radiolarian.

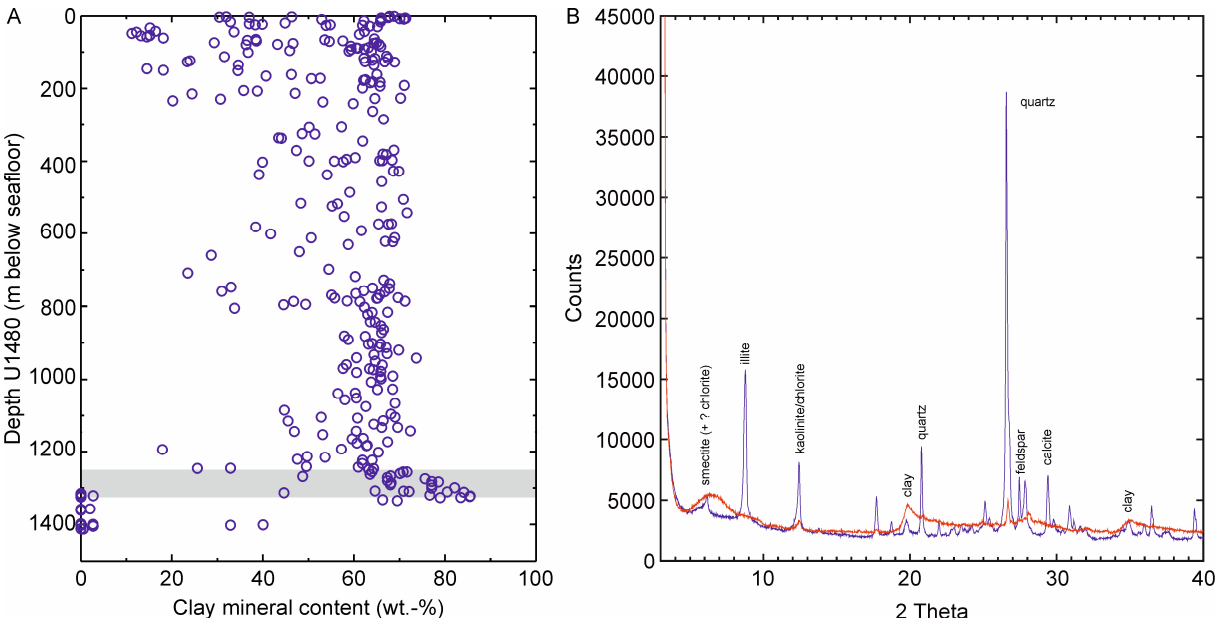

Fig. S3. Results of the shipboard XRD measurements. (A) Relative abundance of clay mineral content at Site U1480. Gray bar indicates depth interval of interest (location of chloride and silica anomalies). (B) Comparative XRD patterns (random powder mounts) of typical silty mudstone of Unit IIC (blue; Site U1480, 1214.24 m below seafloor) and palagonized tuffaceous mudstone (red; Site U1480, 1325.88 m below seafloor) of Unit III. The palagonite composition contrasts drastically with the silty mudstone in the near-absence of crystalline non-clay minerals (quartz, feldspar, and calcite) that are associated with the silt-size fraction. The highly crystalline detrital clays illite and kaolinite that characterize the silty mudstone are also absent in the palagonite sample. The palagonite is composed almost entirely of poorly crystalline expandable clay (with low-intensity broad peaks, corresponding to a smectite or, possibly, an expandable chlorite) and an unknown quantity of amorphous material (palagonite components + biosilica) that is indicated by the elevated background.

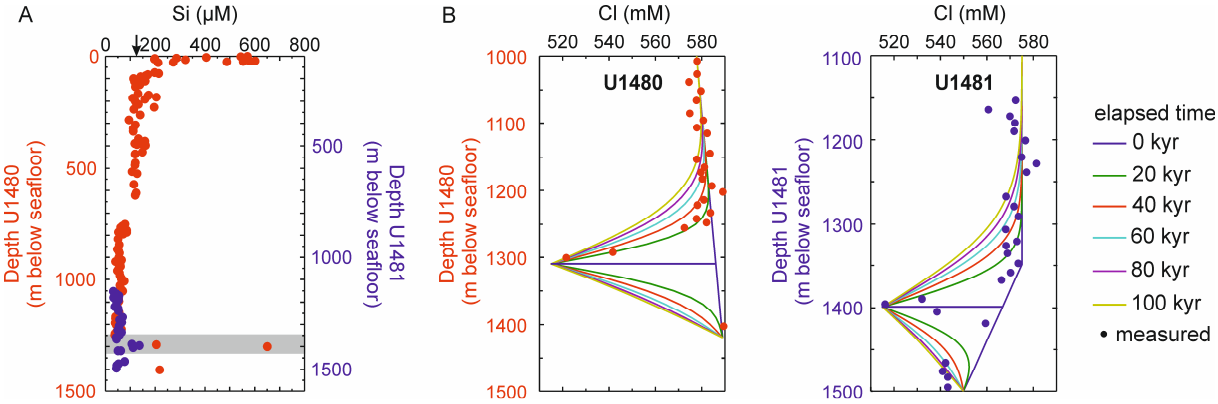

Fig S4. Profiles of dissolved Si and Cl for Sites U1480 (red) and U1481 (blue) in comparison with numerical modeling of Cl diffusion (lines). A) The sharp decrease in chloride within unit III between 1250 and 1330 m below seafloor at Site U1480 and between 1350 and 1450 m below seafloor at Site U1481 (Fig. 2) is accompanied by attendant increases in dissolved silica (to ~650 µM at Site U1480 and to ~140 µM at Site U1481). The chloride concentration of 590 mM measured in a single sample recovered near the sediment/basement interface (Fig. 2) is indicative of alteration reactions in oceanic basement (16). The high hydrostatic effective stress of ~14 MPa at the base of unit III (*16*) suggests that the contribution of interlayer water to the freshening as a laboratory artifact of squeezing smectite minerals (*33*) is negligible. Black arrow shows seawater value of dissolved silica. Gray bar indicates depth interval of interest (location of chloride and silica anomalies). B) Colored lines on the close up view of the Cl profiles are predicted at different times since release of fresh water by a simple diffusion model, showing that the observed anomalies in this zone must be a very recent (<100 kyr) feature.

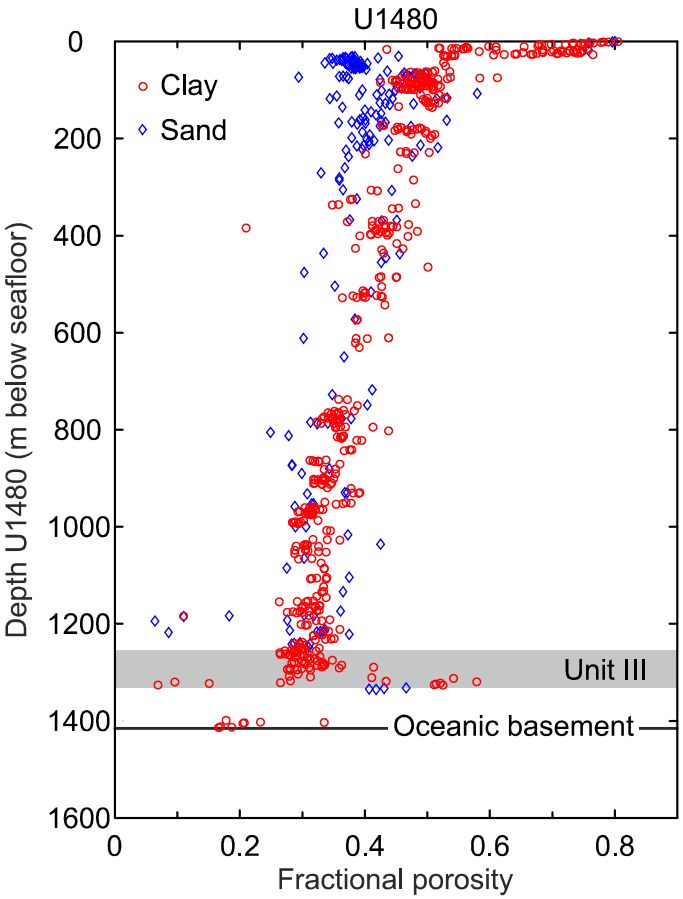

Fig. S5. Depth profile of fractional porosity at Site U1480. Gray area shows the depth interval of unit III at Site U1480 with geochemical anomalies indicating freshening.

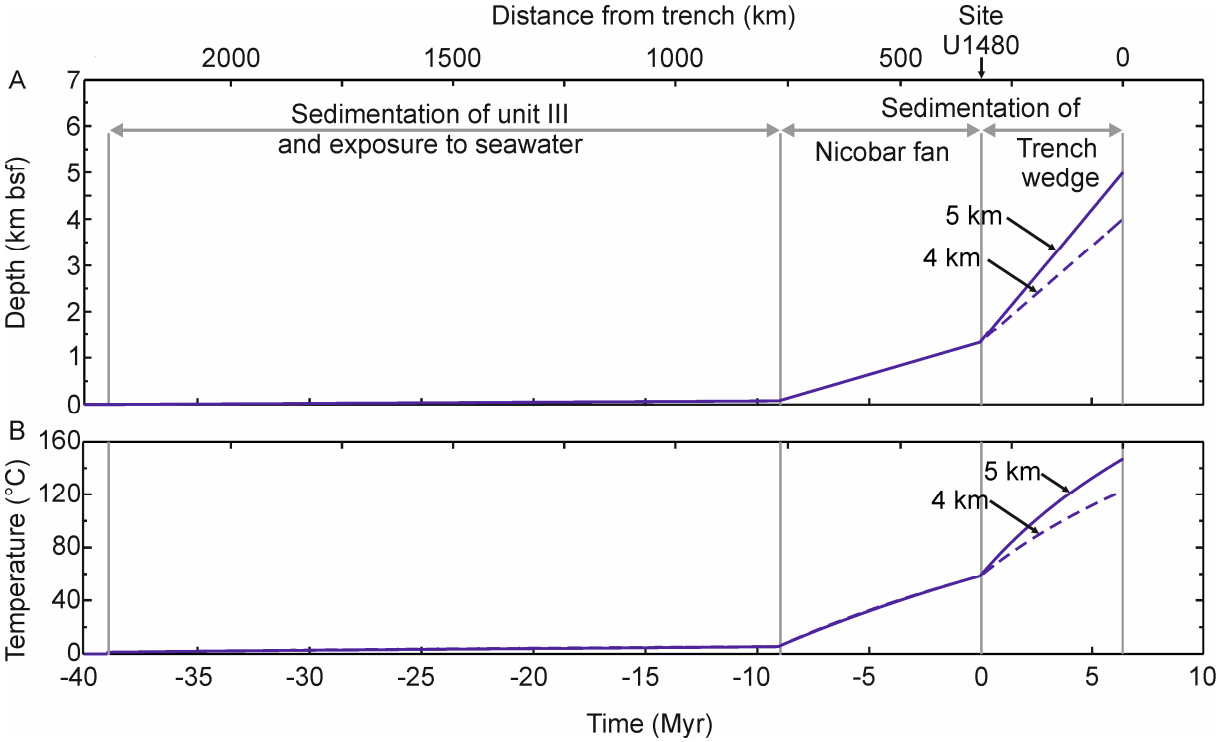

Fig. S6. Reconstructed depth in km below seafloor (A) and temperature (B) history of the base of unit III of Site U1480 since time of deposition (16) to its arrival at the subduction deformation front. The base of unit III has reached a burial depth of ~1327 mbsf and a temperature of ~59°C at 0 Myr, which corresponds to the present time. Based on estimates for the thickness of the trench wedge from seismic reflection data in the trench we utilized final sediment thickness and burial depths of 4 and 5 km for that we predicted temperatures of ~120 and 150°C in the trench, respectively.

Table S1. Summary of input, diagenesis and earthquake parameters from a range of subduction margins, primarily accretionary margins, for comparison with North Sumatra. Margins include those to which the results from this study could be applied. Data taken from and close to drilling transects where available, but supplemented with data (e.g., seismic reflection, heat flow measurements) away from these transects to provide variability along strike where possible. EPR=East Pacific Rise, CNS=Cocos-Nazca Spreading center.

Subduction Zone	**Total input sediment thickness at deformation front (km)**	**Depth of décollement below seafloor at deformation front (km)**	**Temperature, décollement depth at deformation front**	**Reason for elevated temperature, if present**	**Recorded historic earthquakes**	**Evidence of plate boundary slip behavior**	**Drilling of décollement interval in inputs or trench/ deformation front**	**Evidence of dehydration pre-subduction**	**Proposed models: dehydration and earthquake slip**	**References**
Nankai-Muroto	1.2-1.3	0.8-0.95	~50-60°C (~110°C at top basement in trench) Data: Modeling, heat flow probe, borehole measurements	High heat flow from Kinan seamount chain subduction and crustal fluid circulation	Yes (1946)	Yes. Slip confined further landward (beneath forearc basin)	Yes (input site 1173 and trench/frontal thrust sites 1174, 808)	Evidence for minor diagenetic alteration before subduction (sites 1173, 808). Peak dehydration modeled at ~16 km into subduction zone	Major dehydration within subduction zone, updip limit at forearc basin/prism boundary	*42, 45 - 50*
Nankai-Kumano	2.4	0 - 1.4 (note décollement at drilling transect reaches seafloor, likely locally anomalously shallow - décollement deepens rapidly down and along strike)	~60-70°C (using deep décollement position) Data: Modeling, heat flow probe, borehole measurements	High heat flow possibly from crustal fluid circulation. Thickened sediment input	Yes (1944)	Yes. Slip confined further landward (beneath forearc basin)	Yes (input sites C0011, C0012, frontal thrust site C0006)	No	Major dehydration within subduction zone, updip limit at forearc basin/prism boundary	*47, 49, 51 - 55*

Cascadia (43-48°N)	2.5-4	1.7-4 (0-1.35 km above basement)	>100°C (potentially >160°C) at trench within décollement depth sediments. Data: Modeling, heat flow probe	Young oceanic crust (6-8.5 Ma), thick sediment section (rapidly accumulated)	No (large magnitude earthquakes/ tsunami interpreted from geological record)	No	Yes (inner input site 174, but not to top oceanic crust, outer input sites 1023-1029; no trench penetration of décollement depth sediments)	Not recorded from core data (e.g., Site 174), but trench inputs not sampled	High heat flow suggests pre-subduction diagenesis and shallow updip limit, but no groundtruth data available	*56 - 60*
Southern Lesser Antilles: **a) Barbados Ridge drilling transect (15.5°N)** **b) South of 15°N**	a) 0.8-1 b) 1.5-5	a) 0.2-0.3 (0.5-0.6 km above basement) b) Examples: 1.9 in 3.2 km sediment; 3.5 in 5 km sediment	a) <<50°C predicted at trench décollement b) No specific predictions of trench décollement temperature (normal heat flow), but modeling predicts 100°C isotherm 20 km landward of trench in south Data: Borehole measurements, heat flow probe, modeling	a) Localized high heat flow likely related to fluid discharge b) High temperatures may be expected from burial by thick Orinoco fan sediments	No	No	a) Yes (trench sites 676, 1047, 671; inner input sites 1048, 672) b) No	a) Possibly yes, illite:smectite ratio suggests clay diagenesis initiated, however likely fluid related and probably localized (or non-diagenetic origin) b) No groundtruth data available	a) Major dehydration within the subduction zone (potentially peaking 50-75 km landward of deformation front), updip limit landward. b) Thick sediment input suggests early diagenesis and potential shallow updip limit if décollement pore pressure low (mud volcanoes suggest overpressure)	*1, 61 - 71*

Eastern Makran (Pakistan)	1-7.5	1-6 (0-3 km above basement)	~100°Cat trench within décollement depth sediments Data: Modeling, heat flow probe	Burial by gradually accumulated, thick sedimentary section (Indus Fan)	Maybe (1945)	No	No	No	Thick sediment input suggests early diagenesis and shallow updip limit if pore pressure low at décollement	*26, 72*
North Sumatra	4-5	~4 (~0.5 km above basement)	~120-150°C at trench within décollement depth sediments Data: Modeling, heat flow probe, borehole measurements	Burial by gradually accumulated, thick sedimentary section (Nicobar Fan)	Yes (2004)	Yes, slip beneath outer forearc towards trench	Yes (input sites U1480, U1481)	Yes (this study)	This study: Thick sediment section leads to extensive pre-subduction diagenesis and shallow updip limit	This study and references therein; *9, 16, 73, 74*
Eastern Aleutians/ Kodiak-Alaska	~2-4	~1-2 (1-2 km above basement)	80°C modeled at 1.6 km depth (in trench basal sediments) Data: Modeling, borehole measurements	Burial by thick sediment (but rapidly and recently accumulated, >90% deposited in <3 Myr)	Yes (1964)	Yes, apparent shallow slip during 1964	Yes (input site U1417/178 to basement; trench site 180, but does not sample décollement interval)	Modeling predicts dehydration starts outboard of deformation front, but peaks within subduction zone. Diagenesis not reported at U1417	Major dehydration predicted within subduction zone, but evidence for shallow slip	*26, 27, 75 - 78*

Costa Rica (Nicoya-north, Osa-south)	~0.1-0.6	~0-0.4 (décollement often initiates shallow. Deepens rapidly but involvement of upper or lower plate sediments not always clear)	~35-55°C in south (warm CNS), ~5-40°C in north (cool EPR) Data: Modeling, heat flow probe, borehole measurements		Yes	Yes, slip confined further landward, seismicity starts ~60-75 km landward of trench	Yes (input site e.g., 1381, trench sites e.g., 1039, 1040, 1253, 1414)	No	Dehydration within subduction zone (onset predicted ~20-45 km landward of trench). Updip limit ~60-75 km landward of trench	*79 - 85*
Japan Trench	~0.4-0.5	~0.1-0.4 (typically ~0.1 km above basement)	≤20°C at deformation front Data: Borehole measurements		Yes (2011)	Yes, slip beneath outer forearc to trench	Yes, outermost forearc drilled, but not to top oceanic crust	No	Dehydration within subduction zone. Slip to trench, driven by weak clay	*25, 86 - 89*